Cascades of Velocity and Temperature Fluctuations in Buoyancy-Driven Thermal Turbulence

Chao Sun, Quan Zhou, and Ke-Qing Xia

Department of Physics, The Chinese University of Hong Kong, Shatin, Hong Kong, China

(Received 26 May 2006; published 3 October 2006)

Direct multipoint measurements of the velocity and temperature fields have been made in a turbulent Rayleigh-Bénard convection cell. In the central region of the cell it is found that both velocity and temperature exhibit the same scaling behavior that one would find for the velocity and for a passive scalar in homogeneous and isotropic Navier-Stokes turbulence. This is despite the fact that energy is pumped into the system vertically via buoyancy. Near the cell's sidewall where thermal plumes abound, vertical velocity and temperature exhibit different scalings. A model that takes into account both buoyancy and energy dissipation is proposed and its predictions agree well with the sidewall experimental results.

DOI: 10.1103/PhysRevLett.97.144504 PACS numbers: 47.27.−i, 05.45.−a, 44.25.+f

An important class of fluid motion found ubiquitously in nature is buoyancy-driven turbulent flows. A model system to study this type of flow is turbulent Rayleigh-Bénard (RB) convection. An important issue in the study of fluid turbulence is to determine the dynamics that drive the cascades of turbulent velocity and temperature fluctuations from large to small scales. Different dynamics may be manifested as different scaling laws for the velocity and temperature structure functions (SF), which are the statistical moments of the velocity and temperature differences over a distance r, i.e., $S_p(r) = \langle|\delta V_r|^p\rangle$ and $R_p(r) = \langle|\delta T_r|^p\rangle$. In the RB system the situation is more complicated because the smallest scale is associated with the thermal boundary layers that detach to form thermal plumes that cluster or organize to form the large scale flow that then cascades to small scales. This small-to-large-to-small behavior makes the RB problem even more challenging and interesting. Based on dimensional arguments, Bolgiano and Obukhov (BO59) [1,2] proposed in 1959 that for stably stratified convection two different dynamics control the cascades of turbulent velocity and temperature fluctuations within the usual inertial range which is divided by the Bolgiano length l_B. For $r > l_B$ buoyancy is the dominant force and one expects to observe $S_p(r) \sim r^{3p/5}$ and $R_p(r) \sim r^{p/5}$; below l_B inertia becomes the driving force and one expects to see for the velocity the usual Kolmogorov scaling (K41) [3] and for the temperature the Obukhov-Corrsin scaling (OC) [4,5] predicted for a passive scalar. Over the years a number of experimental and numerical studies of RB convection appear to have observed the BO59 [6–14] and several theoretical models [15–17] also found BO59 for this system. On the other hand, there are also theoretical and numerical evidences that cast doubt on its existence [18–22]. In the studies that appear to have shown BO59, some are based on very limited scaling range or data resolution while many others are based on data obtained in the time or frequency domain. To relate the time domain results to the theoretical predictions made for the space domain requires the use of the Taylor frozen-turbulence hypothesis, the validity of which demands that turbulent velocity fluctuations be much smaller than the mean flow velocity. However, it is known that the mean velocity is either zero or is comparable to the rms velocity, depending on the place in RB convection cell.

This Letter reports multipoint measurements of the velocity and temperature fields in turbulent convection, from which real-space SFs are obtained. The experiment was conducted in a RB convection cell which has been described in detail elsewhere [23]. Briefly it is a vertical cylinder of height $H = 19.3$ cm and diameter $D = 19.0$ cm, with upper and lower copper plates and Plexiglas sidewall. During the velocity and temperature measurements the convection cell was placed inside a thermostat box that was kept at the mean temperature (40 °C) of the convecting fluid, which was water. The control parameters of the system are the Rayleigh number Ra ($= \alpha g H^3 \Delta/\nu\kappa$), and the Prandtl number Pr ($= \nu/\kappa$), where g is the gravitational acceleration, Δ the temperature difference across the cell, and α, ν, and κ, respectively, the thermal expansion coefficient, the kinematic viscosity, and the thermal diffusivity of the fluid. The velocity measurement was made at Ra $= 7.0 \times 10^9$ and temperature measurement at Ra $= 1.0 \times 10^{10}$ while Pr$= 4.3$ in both cases. At these values of Ra and Pr the Kolmogrov scale $\eta = H\mathrm{Pr}^{1/2}/(\mathrm{Ra}Nu)^{1/4} \approx 0.4$ mm and the Bolgiano scale $\ell_B = HNu^{1/2}/(\mathrm{Ra}\,\mathrm{Pr})^{1/4} \approx 5$ mm [8]. It is well known that the sidewall region of the cell is dominated by thermal plumes, whereas the central region has relatively few plumes [24]. This suggests that velocity and temperature may exhibit different behavior in the two regions. We thus selected an area of 4×4 cm^2 in the cell center and another of 4 cm high and 2 cm wide near the sidewall (at midheight with its edge 1 cm from the wall) for high-resolution measurements of both velocity and temperature.

A pair of thermistors 300 μm in size with a time constant of 10 ms are used in the temperature measurements. Each thermistor is mounted on a stainless steel tube (di-

ameter 1 mm), which is similar to that depicted in Ref. [25] except that in the present case one thermistor is fixed while the other can traverse vertically via a motorized translation stage (precision 0.01 mm). The thermistors are connected to separate ac bridges modulated by a sinusoidal signal of 1 kHz. The bridge outputs are demodulated by lock-in amplifiers and then digitized by a dynamical signal analyzer [12]. In the experiment the vertical separation r between the thermistors varied from 0.5 mm to 9 cm. For a given r, two simultaneous temperature time series each consisting of 1 152 000 data points are acquired at a sampling rate of 32 Hz.

The multipoint velocity field was measured using the particle image velocimetry (PIV). The PIV system and the selection criteria for operating parameters have been described in detail elsewhere [23]. In the present work, the seed particles are 50-μm-diameter polyamid spheres (density 1.03 g/cm^3) and the laser light-sheet thickness is $\sim$0.5 mm. The spatial resolution is 0.66 mm, which corresponds to 61×61 velocity vectors in the central measuring area and 61×30 vectors in the sidewall measuring area. A water-filled square-shaped jacket made of flat glass plate is fitted to the outside of the sidewall [24], which greatly reduced the distortion effect to the PIV images caused by the curvature of the cylindrical sidewall. Denote the laser-illuminated plane as the xz plane, then the horizontal velocity component $u(x, z)$ and the vertical one $w(x, z)$ are measured. Each measurement lasted 1 hr in which a total of 7500 vector maps were acquired (sampling rate 2 Hz). To obtain high-order SFs with good statistics recall that if the flow is locally homogeneous then $S_p(\mathbf{r}) = \langle |V(\mathbf{x} + \mathbf{r}) - V(\mathbf{x})|^{\mathbf{p}} \rangle$ is independent of the position $\mathbf{x}$. This will be the case if the n-point joint probability density function (PDF) of different δV_r for varying values of $\mathbf{r}$ is independent of $\mathbf{x}$ [26]. Using the measured velocity we calculated PDF for $n = 2$ and 3 for various values of $\mathbf{r}$ and $\mathbf{x}$ and found that they all collapse on top of each other, except some scatter near the tails which are probably due to the limited statistics. More rigorous test involving multipoint PDF with $n > 3$ is certainly needed to fully validate the local homogeneity of the system. However, if we take this preliminary result as evidence that the flow is approximately locally homogeneous, then each velocity difference $V(\mathbf{x} + \mathbf{r}) - V(\mathbf{x})$ for a fixed $\mathbf{r}$ and a given $\mathbf{x}$ within the measuring area makes a distinct contribution to the ensemble average. Each of the 7500 vector field represents a realization of the flow configuration so that it also makes a distinct contribution to the ensemble average. We thus have 27 907 500 ($61 \times 61 \times 7500$) and 13 725 000 ($61 \times 30 \times 7500$) velocity points for the central and sidewall regions, respectively. These correspond to 24.7 to 15.1 M pairs of velocity differences in the center and 12.6 to 3.72 M in the sidewall for the smallest and largest r in the inertial range, respectively. With the measured 2D velocity field, we can calculate both longitudinal and transverse SFs, i.e., for separations along and perpendicular to the velocity direction, respectively. For w these are defined as $S_p^{L,w}(r) = \langle |w(x, z + r) - w(x, z)|^p \rangle$ and $S_p^{T,w}(r) = \langle |w(x + r, z) - w(x, z)|^p \rangle$, respectively. Those for u can be similarly defined. The upper panel of Fig. 1 plots in log-log scale $S_p^{L,u}(r)/r^{p/3}$ and $R_p(r)/r^{p/3}$ vs r at cell center for $p = 1$ to 8. The compensated plot shows the quality of the SFs and their progressive deviation from the K41 prediction with increasing p. To show the level of convergence of these SFs we plot in the lower panel their kernels for $p = 6$ and 8. Figure 1 shows that the SF for both velocity and temperature exhibit good scaling over the same range of scales which are larger than l_B and smaller than the integral scale L ($\sim$3 cm). As scaling is generally expected only for $r > 10\eta$ which roughly corresponds to l_B in the present case, so the inertial range here is, coincidentally, $l_B < r < L$. It is found that in general temperature has longer scaling range than velocity and that near the sidewall the range of scaling is also longer than it is at cell center.

Table I lists the scaling exponents ζ_p of velocity and ξ_p of temperature SFs of orders $p = 1$ to 8, where $\zeta_p^{L,w}$ is that of the longitudinal SF of w, etc. We first discuss the central region results. When these are compared with well-known experimental results from Navier-Stokes turbulence for velocity and passive scalars [27,28], we find extremely good agreement. Table I also shows clearly that the exponents of the various velocity SFs in the center are essentially the same within experimental uncertainty. This implies that the velocity field is isotropic in the central region. In isotropic flow the second order longitudinal and

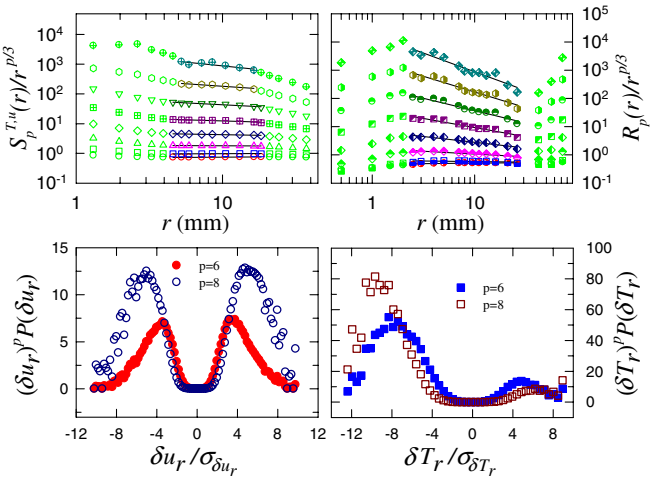

FIG. 1 (color online). Upper panel: Compensated velocity and temperature SFs of order 1 to 8 (from bottom to top) measured at central region as a function of r. Data inside and outside of the scaling range are represented by different colors and the lines represent power-law fits to data in the inertial range. Lower panel: Integral kernels of SF at the smallest r in inertial range for $p = 6$ and 8 (the vertical scale for $p = 8$ has been reduced by 10 and 50 times for the velocity and temperature, respectively).

TABLE I. Exponents of structure functions of order $p = 1$ to 8. Columns 2–6: Center results for longitudinal (L) and transverse (T) SF of the vertical (w) and horizontal (u) velocities and the temperature. Columns 7–9: Sidewall results for the vertical velocity longitudinal and horizontal velocity transverse SF and the temperature.

	Center					Sidewall		
p	$\zeta_p^{L,w}$	$\zeta_p^{T,w}$	$\zeta_p^{T,u}$	$\zeta_p^{L,u}$	ξ_p	$\zeta_p^{L,w}$	$\zeta_p^{T,u}$	ξ_p
1	0.35 ± 0.01	0.35 ± 0.01	0.36 ± 0.01	0.36 ± 0.01	0.37 ± 0.01	0.40 ± 0.01	0.38 ± 0.01	0.33 ± 0.01
2	0.68 ± 0.01	0.68 ± 0.01	0.68 ± 0.01	0.68 ± 0.01	0.63 ± 0.01	0.78 ± 0.01	0.72 ± 0.01	0.59 ± 0.01
3	0.99 ± 0.01	1.00 ± 0.01	0.98 ± 0.01	0.98 ± 0.01	0.80 ± 0.01	1.14 ± 0.01	1.01 ± 0.01	0.80 ± 0.01
4	1.25 ± 0.02	1.27 ± 0.02	1.26 ± 0.02	1.25 ± 0.02	0.93 ± 0.01	1.48 ± 0.02	1.27 ± 0.02	0.97 ± 0.01
5	1.53 ± 0.03	1.51 ± 0.03	1.52 ± 0.03	1.53 ± 0.03	1.03 ± 0.01	1.78 ± 0.03	1.52 ± 0.04	1.13 ± 0.02
6	1.81 ± 0.04	1.73 ± 0.04	1.76 ± 0.04	1.76 ± 0.04	1.12 ± 0.02	2.03 ± 0.04	1.70 ± 0.06	1.31 ± 0.02
7	2.02 ± 0.06	1.96 ± 0.06	2.00 ± 0.06	1.99 ± 0.06	1.22 ± 0.04	2.21 ± 0.06	1.94 ± 0.08	1.52 ± 0.04
8	2.30 ± 0.10	2.09 ± 0.10	2.14 ± 0.10	2.07 ± 0.10	1.33 ± 0.05	2.36 ± 0.08	2.05 ± 0.13	1.77 ± 0.05

transverse SFs are related as $S_2^T(r) = S_2^L(r) + (r/2) \times (\partial S_2^L/\partial r)$ [26]. Using $\zeta_2 = 0.68$ from the present work we have $S_2^T/S_2^L = 1 + \zeta_2/2 = 1.34$. For values of r in the inertial range, we find that $S_2^T(r)/S_2^L(r)$ varies from 1.28 to 1.32 with a mean of 1.31 for w, and from 1.32 to 1.36 with a mean of 1.34 for u. An equivalent criterion for local isotropy is that the longitudinal integral scale L_{11} is twice of the transverse one L_{22}, which are obtained by integrating the longitudinal and transverse autocorrelation functions of the velocity respectively [26]. Here we find in the center region $L_{11} = 28.2$ mm and $L_{22} = 14.4$ mm.

A comparison of the measured exponents with various theoretical predictions is shown in Fig. 2 [the predictions of K41 for the velocity and OC for passive scalars are the same $(p/3)$]. The figure shows that the present results do not support BO59 and that they are closer to the classical predictions. However, full agreement with the classical results are not expected because they do not consider the intermittency effect. The hierarchy models of She and Lévêque (SL94) [29] for velocity, and of Ruiz-Chavarria *et al.* (RCBC96) [28] for passive scalars seem to account the intermittency effect well; their predictions are plotted also in Fig. 2. The excellent agreement between the models and experiment suggests that the velocity and temperature in the central region of the convection cell exhibit the same behavior as the velocity field and a passive scalar would behave in homogeneous and isotropic Navier-Stokes turbulence. This result appears at first counterintuitive since the flow is driven by buoyancy in the vertical direction. Indeed, even in the central region temperature shows stronger correlation with the vertical velocity than with the other two velocity components [22]. However, one may argue that isotropy may be realized by pressure that can rapidly redistribute energy among different velocity components [17]. It is also argued in [18,19] that temperature should be passive. Numerically it was found in [20] that velocity and temperature follow K41 scaling, while in [21] K41 was found for velocity. Experimentally it was found in

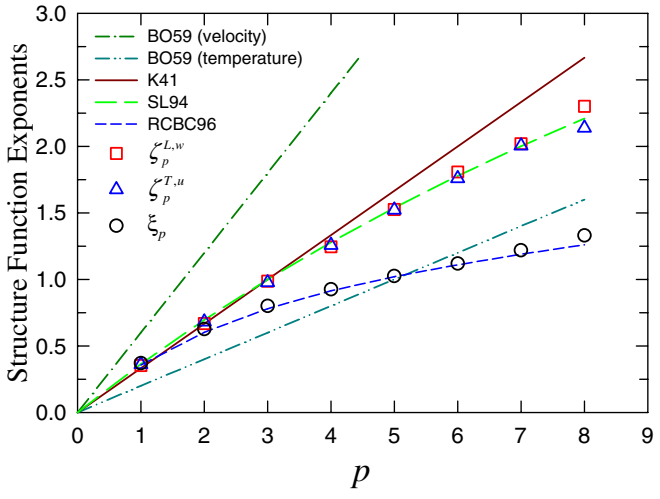

FIG. 2 (color online). Comparison of velocity and temperature SF exponents measured at cell center with various model predictions.

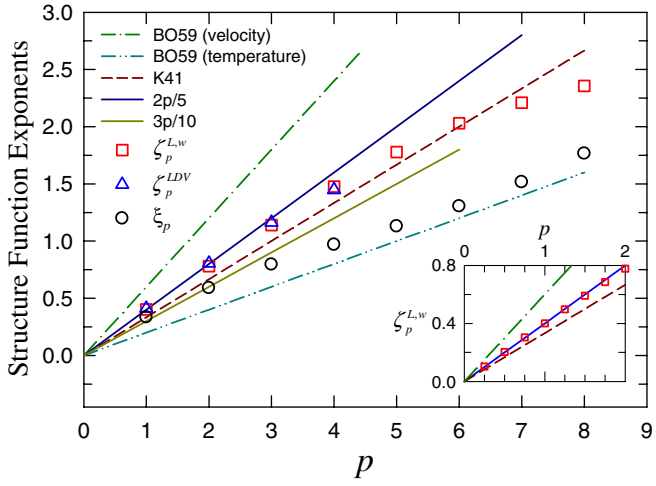

FIG. 3 (color online). Comparison of velocity and temperature SF exponents measured at sidewall with model predictions. Inset: Exponents of fractional-order velocity SF for p between 0 and 2 (lines and symbols are the same as in the main figure).

[30] that temperature is active but for $\mathrm{Ra} > 10^{10}$ it may become progressively passive. We note that our results do not agree with the prediction of the Kraichnan model for passive scalars [31], as it is not expected to be applicable here.

Because of the limited size of the sidewall measuring area in the horizontal direction we calculate only velocity differences along the vertical direction, i.e., the longitudinal and the transverse SFs $S_p^{L,w}(r)$ and $S_p^{T,u}(r)$ for the vertical and horizontal velocities, respectively. It is seen from Table I that the sidewall exponents for the horizontal velocity are consistent with those in the central region. The exponents for the vertical velocity and temperature are very different from those in the central region and follow neither BO59 nor the K41/SL94 predictions, which is further shown in Fig. 3. How can we understand these results? The basic assumption that leads to BO scaling is that for scales larger than l_B viscous dissipation is negligible comparing to the buoyancy and the cascades of velocity and temperature variances are determined by the temperature dissipation rate ϵ_θ, the buoyancy αg, and the scale r of velocity and temperature variations [1,2]. Here we argue that while buoyancy is important in the plume-dominated sidewall region, energy dissipation ϵ_v cannot be neglected, so that the cascades of velocity and temperature variations depend also on ϵ_v, in addition to $\alpha g \triangle$, ϵ_θ, and r. Dimensional analysis then leads to $\langle(\delta V_r)^p\rangle \sim (\alpha g \triangle \epsilon_v)^{p/5} r^{2p/5}$ and $\langle(\delta T_r)^p\rangle \sim (\alpha g \triangle \epsilon_v)^{-p/10} \times \epsilon_\theta^{p/2} r^{3p/10}$, which are shown in Fig. 3. As these results do not consider the intermittency effect, they are not expected to be correct for high-order SFs. So we examine the fractional-order SFs of small p. These are shown in the inset of Fig. 3 for velocity SFs of $p \leq 2$. The present model is seen to agree well with the experimental results which are clearly different from both BO59 and K41. Clearly, more detailed and systematic test of the model is needed.

As we remarked earlier many of the previous experimental measurements that showed BO scaling were made in time or frequency domain and Taylor hypothesis was invoked to connect them to theoretical predictions. As an example, we consider a previous experimental result. The data [11] were vertical velocities measured by laser Doppler velocimetry (LDV) near the sidewall of a convection cell similar to the present one and its frequency power spectrum exhibited BO scaling [11]. Here we use a local Taylor hypothesis method that uses a local velocity averaged over the integral time scale of the flow to convert velocity from time domain to space domain [32]. As this method was developed for the hot-wire data, we first resampled our LDV data with equal-time interval before using the method. The exponents ζ_p^{LDV} of the longitudinal SF calculated based on the converted velocity is shown in Fig. 3, which is seen to agree excellently with the present results instead of either BO59 or K41 (only $p \leq 4$ are obtained because of the limited sample size of the LDV data).

We thank X. D. Shang for making the LDV data available to us and E. S. C. Ching for stimulating discussions. This work was supported by the Hong Kong RGC (Grant No. CUHK403705). K. Q. X. acknowledges the support of the Croucher Foundation of Hong Kong.

[1] R. Bolgiano, J. Geophys. Res. **64**, 2226 (1959).
[2] A. M. Obukhov, Dokl. Akad. Nauk SSSR **125**, 1246 (1959).
[3] A. N. Kolmogorov, Dokl. Akad. Nauk SSSR **32**, 16 (1941).
[4] A. M. Obukhov, Izv. Akad. Nauk. SSSR Geogr. Geofiz. **13**, 58 (1949).
[5] S. Corrsin, J. Appl. Phys. **22**, 469 (1951).
[6] X.-Z. Wu *et al.*, Phys. Rev. Lett. **64**, 2140 (1990).
[7] P. Tong and Y. Shen, Phys. Rev. Lett. **69**, 2066 (1992).
[8] S. Cioni *et al.*, Europhys. Lett. **32**, 413 (1995).
[9] S. Ashkenazi and V. Steinberg, Phys. Rev. Lett. **83**, 4760 (1999).
[10] J. J. Niemela *et al.*, Nature (London) **404**, 837 (2000).
[11] X.-D. Shang and K.-Q. Xia, Phys. Rev. E **64**, 065301(R) (2001).
[12] S.-Q. Zhou and K.-Q. Xia, Phys. Rev. Lett. **87**, 064501 (2001).
[13] E. Calzavarini *et al.*, Phys. Rev. E **66**, 016304 (2002).
[14] T. Mashiko *et al.*, Phys. Rev. E **69**, 036306 (2004).
[15] I. Procaccia and R. Zeitak, Phys. Rev. Lett. **62**, 2128 (1989).
[16] V. S. L'vov, Phys. Rev. Lett. **67**, 687 (1991).
[17] V. Yakhot, Phys. Rev. Lett. **69**, 769 (1992).
[18] B. I. Shraiman and E. D. Siggia, Phys. Rev. A **42**, 3650 (1990).
[19] B. Castaing, Phys. Rev. Lett. **65**, 3209 (1990).
[20] S. Grossmann and D. Lohse, Phys. Rev. Lett. **67**, 445 (1991).
[21] R. M. Kerr, J. Fluid Mech. **310**, 139 (1996).
[22] E. S. C. Ching *et al.*, J. Turbulence **5**, 027 (2004).
[23] C. Sun *et al.*, Phys. Rev. E **72**, 026302 (2005).
[24] H.-D. Xi *et al.*, J. Fluid Mech. **503**, 47 (2004).
[25] S.-Q. Zhou and K.-Q. Xia, Phys. Rev. E **63**, 046308 (2001).
[26] S. B. Pope, *Turbulent Flows* (Cambridge University Press, Cambridge, UK, 2000).
[27] R. A. Antonia *et al.*, Phys. Rev. A **30**, 2704 (1984).
[28] G. Ruiz-Chavarria *et al.*, Physica D (Amsterdam) **99**, 369 (1996).
[29] Z.-S. She and E. Lêvêque, Phys. Rev. Lett. **72**, 336 (1994).
[30] A. Belmonte and A. Libchaber, Phys. Rev. E **53**, 4893 (1996).
[31] R. H. Kraichnan, Phys. Rev. Lett. **72**, 1016 (1994).
[32] J. F. Pinton and R. Labbé, J. Phys. II (France) **4**, 1461 (1994).